Numerical Methods in Civil Engineering, 6-4 (2022) 78-97

Numerical Methods in Civil Engineering

Journal Homepage: https://nmce.kntu.ac.ir/

Evaluation of the seismic performance of isolated electrical transformers under pulse-like excitations

Mohammad Mahmoudi*, Abbas Ghasemi, Shahriar Tavousi Tafreshi*****

ARTICLE INFO

RESEARCH PAPER

Article history:
Received:
December 2021.
Revised:
February 2022.
Accepted:
February 2022.

Keywords:
Electrical transformer,
Three-dimensional isolation,
Failure performance evaluation,
near-fault pulse-like ground motions,
fragility curves

Abstract:

Damage sustained by electrical transformers in past strong earthquakes led to irrecoverable and severe economic losses. The seismic performance evaluation is associated with the loss of proper functioning of transformers. This study deals with modeling existing isolated electrical transformer structures to evaluate the effects of variables that may affect the seismic performance and dynamic characteristics. The results probabilistically determine the seismic performance acceptability of study isolated electrical transformer structures based on the impact of key structural response parameters on the seismic performance of the transformer. Analyses of systems for a wide range of parameters are performed. The effects of horizontal and vertical near-fault pulse-like ground motions, the displacement capacity of the seismic isolation system, limit states of electrical bushings, and details of the isolation system design are considered. Also, the probability of failure of the transformer under the near-fault excitations with pulse-like characteristics is investigated. The results of the research showed that the three-dimensional seismic isolation system has a significant effect on improving the seismic performance of the system for a large number of parameters and can be further effective compared with horizontal-only seismic isolation, offering the lowest probabilities of failure for all cases of transformer and isolation system parameters.

1. Introduction

Electrical transformers are the primary members of the lifeline engineering systems. They are meant to reserve electricity continually and have a low vulnerability to disasters. Empirical observations of past earthquakes illustrate that the electrical equipment was severely damaged by the earthquake [1–5]. Damage to electrical infrastructure leads to great economic losses.

Estimated instant economic losses in earthquakes such as the 1993 Kushiro-Oki, Japan, 1994 Northridge, USA, 1995 Kobe, Japan, 1999 Kocaeli, Turkey, and the 1999 Chi-Chi, Taiwan caused hundreds of millions of dollars in damage to electrical equipment [6,7].

The electricity network is made up of power stations, transmission lines, and distribution lines. The electric transformers used to raise and lower voltages lie between these elements [8]. The main members of electrical transformers are high voltage bushings that establish the electrical connection between the high voltage lines and the transformer [9]. Bushings are most vulnerable to seismic ground motions [7,8]; Therefore, a lot of research has been done to reduce the vulnerability of the bushings and transformers in various scientific academies [8,10-13]. Numerous studies have been performed to evaluate the seismic performance of transformers using the horizontal seismic isolation system. The results showed that the relative displacement and acceleration in the bushing and transformer bodies are reduced in the horizontal direction [8,11,12,14-16]. These studies did not consider the effect of vertical ground motion on the performance of the horizontal isolation system. They also showed that vertical ground

* *Ph.D. Candidate, Department of Civil Engineering, Faculty of Civil and Earth Resources Engineering, Central Tehran Branch, Islamic Azad University, Tehran, Iran.*
** *Corresponding author: Assistant Professor, Department of Civil Engineering, Faculty of Civil and Earth Resources Engineering, Central Tehran Branch, Islamic Azad University, Tehran, Iran. Email: abb.ghasemi@iauctb.ac.ir*
*** *Assistant Professor, Department of Civil Engineering, Faculty of Civil and Earth Resources Engineering, Central Tehran Branch, Islamic Azad University, Tehran, Iran.*

motion in the horizontal isolation system does not decrease. Earlier studies on the assessment of the seismic performance of seismically isolated electrical power transformers [17,18] utilized FEMA P695 [19] procedures with the following limitations:

The study only considered far-field motions. However, some considered sites in the transformer performance evaluation are near active faults, so near-fault pulse-like ground motions (see Section 11.4.1 of ASCE/SEI 7-16 [20] standard for identification) should have been considered. Such motions often lead to larger isolator displacement capacity [21] and, therefore, may affect the failure performance evaluation.

This paper investigates the limitations of past studies by considering performing representative analyses with near-fault pulse-like ground motions [22,23] and evaluates the near-fault pulse-like excitations on the probability of transformer failure. It also compares the acceleration at the center of mass of the bushing in various situations, including fixed base and horizontal isolation only, and a three-dimensional seismic isolation system in near-fault pulse-like ground motions.

The selected transformers are the ones with 420 kip weight and an inclined (20 degrees) bushing of 4.3 Hz or 7.7 Hz or 11.3 Hz frequency (W=320 or 420 or 520 kip, f_{AI}=4.3 or 7.7 or 11.3 Hz). In its non-isolated version, the transformer model has inherent damping of 3% critical in all its modes. Inherent damping was realized in the analysis model by adding translational and rotational viscous damping elements at selected locations. When isolated, the transformer model was placed on top of the seismic isolation model and interconnected without any specification for global damping to avoid affecting the behavior of the isolation system.

This paper provides numerical modeling of a three-dimensional isolation system with a rocking motion and compares the seismic performance of three-dimensional isolated transformers with isolated horizontal-only isolated transformers or non-isolated transformers. The horizontal isolation includes triple FP isolators and the vertical isolation includes a spring-damper device.

This paper presents procedures for the analysis and results of an analytical study of the performance of electrical transformers with particular emphasis on comparing the options of a non-isolated transformer to one isolated only in the horizontal direction or a transformer with a three-dimensional isolation system with rocking considering near-fault pulse-like ground motions.

In this study, in numerical analysis, the vertical ground motion is considered simultaneously with the horizontal ground motion. The study is based on Incremental Dynamic Analysis (IDA) [24]. The numerical model of the analyzed transformers is based on the information obtained from the test of the electrical transformer equipment [5]. Bushing acceleration limits were selected to evaluate transformer failure using field observations and empirical fragility data in past earthquakes [25-28].

One of the most important objectives of this study is to develop fragility curves in the near-field pulse-like ground motions and compare the results with the far-field motions. In all cases, the fragility curve is compared with the non-isolated structure to investigate the effect of seismic isolation in different states on the probability of failure. Also, various other factors such as increasing the displacement capacity of the horizontal isolation, inclined or vertical bushing, the weight of transformers, and different frequencies of the as-installed bushing in the probability of failure are examined.

Incremental dynamic analysis was performed using the near-fault pulse-like ground motions for the three cases of a bushing as-installed frequencies of the 320 or 420, or 520 kip transformers without and with isolators of displacement capacity $D_{Capacity}$ = 17.7 or 27.7 or 31.3 inches. This article evaluates the near-fault ground motions on the displacement capacity of seismic isolation systems with pulse-like characteristics.

2. Principles for failure performance evaluation of isolated transformers

The failure performance evaluation is based on FEMA P695 provisions for collapse performance evaluation. These provisions mandate performing IDA and finding the collapse of the analyzed structure and failure of its critical components by seismic simulation [29-35].

The procedure followed is to conduct IDA to obtain data on the number of failures for each level of seismic intensity considered. In this paper, failure is considered either when the maximum value of acceleration at the center of mass of the upper part of the bushing in the transverse or the longitudinal directions reaches a determined limit or when the isolation system fails by exceeding the horizontal or the vertical (uplift) displacement capacity, whichever happens first. The ground motion intensity is measured in terms of the peak ground acceleration (PGA), or per the vocabulary used in the provisions by IEEE (2005) [36], the zero-period acceleration ZPA.

The 5%-damped high and moderate response spectra required by IEEE are illustrated in Figure 1. The corresponding spectra in the vertical direction are the same shape as the horizontal spectra but scaled in amplitude by a factor of 0.8.

IDA analysis is performed for a set of ground motions, each containing horizontal and vertical components as originally recorded and progressively increased in intensity while sustaining the principal ratio of peak vertical to peak

horizontal acceleration. The intensity is specified as the peak value of the horizontal ground acceleration, the PGA. Failure is specified when either the acceleration reaches a limit based on calibration of the model utilization field, empirical data (1g or 2g in the transverse direction and 5g in the longitudinal bushing direction), or the lateral displacement of the isolators exceeds the stability limit of the isolators, or the vertical isolation system fails in tension (uplift), whichever happens first. The fragility curves demonstrate the probability of failure versus the PGA, where the probability of failure is specified at each PGA level as the number of analyses that led to failure divided by the total number of analyses.

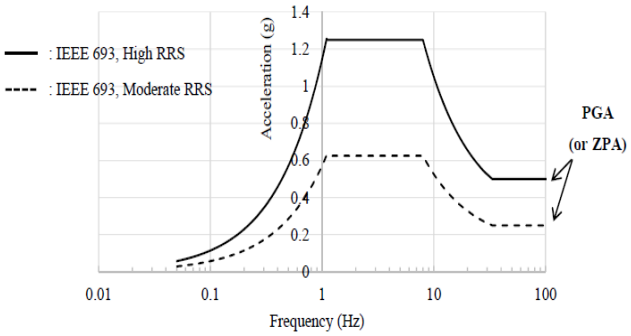

Fig. 1: Moderate and high required response spectra per IEEE 693 (5% damped)

The PGA was selected as the measure of seismic intensity in the scaling of ground motions used in the incremental dynamic analysis for constructing fragility curves. While many studies of seismic assessment of electrical transformers have used the PGA as a measure of seismic intensity [37], the spectral acceleration at the fundamental period $Sa(T_1)$ of the analyzed structure is thought to be a more appropriate measure of intensity and has been used in building performance studies. Kitayama and Constantinou (2018) [38,39] used spectral acceleration at the fundamental period as the measure of ground motion intensity for seismically isolated structures. The selection of the seismic intensity measure affects the scaling of the motions for analysis and accordingly affects the result.

Note that the fragility curves presented are based on the use of the PGA for the measure of ground motion intensity. These differences are from the approach stated in FEMA P695 (2009), where the intensity is measured by the spectral acceleration at the fundamental period of the studied system. Finally, in this study, the reasons for choosing PGA as the intensity measure are:

1) PGA (or ZPA) is the ground motion intensity measure typically used in the fragility analysis of electrical equipment [37,40].

2) It facilitates the utilization of the IEEE 693 spectra, which are determined by PGA (or ZPA) and dissimilar to the ASCE 7 (2010) spectra applied to building design which are described by the spectral acceleration values at 0.2 sec and 1.0 sec.

3) It permits the suggestion of fragility analysis results when the analyzed system has two different vibration modes at two very different frequencies in horizontal and vertical directions.

4) The results of fragility curves can be used in any location, and they only depend on PGA.

In the fragility analysis, PGA_F and β are calculated [39,40]. PGA_F is the measure of intensity (PGA) for which at least 50% of the analyses failed (is the value of PGA for which the probability of failure is 0.5), and the dispersion factor β is calculated as the standard deviation of the natural logarithm of the values of PGA causing failure of the transformer (failure of bushings or the collapse of isolator).

It is necessary to mention that the number of analyses is determined by the rate of increase of PGA in each time step. Also, in this study, the number of ground motions is 40. The analytical fragility curve (cumulative distribution function or CDF) representing the empirical data is calculated as:

$$CDF(x) = \int_0^x \frac{1}{s\beta\sqrt{2\pi}} exp\left[\frac{(\ln s - \ln PGA_F)^2}{2\beta^2}\right] ds \qquad (1)$$

The fragility curves present information on the probability of failure for specific earthquake intensity levels, as measured by the PGA. This information is very effective and has been obtained from numerous dynamic analyses.

3. Modeling of isolated transformers for failure evaluation

3.1 Modeling of bushings

This section describes the modeling of the bushings to evaluate the failure of transformers. Bushings are among the major components of electrical transformers. A bushing's damage or failure is considered a transformer failure [41]. This model uses the results obtained by Kong [42] and Fahad [43], who tested the specifications of bushings installed in different conditions. In particular, the rotational and vertical frequency of the bushing must be considered in their installed condition and accounting for the effects of the flexibility of the supporting plate.

Data from the studies by Kong and Fahad For three types of bushing including geometric features, masses, and frequencies of free vibration when installed fixed (f_{Fix}) and when installed connected to a flexible plate (called as installed frequency, (f_{AI}). Table 1 shows information about the specifications of three different bushings.

Table 1: Characteristics of the tested bushing

	Unit	Bushing 3	Bushing 6	Bushing 8
Voltage capacity	kV	550	196/230	550
Total height	in	244.8	151.4	255.2
Length over mounting flange: H_{UB}	in	194.8	91.4	190.2
Length below mounting flange: H_{LB}	in	50	60	65
Total weight	lbs	2810	4330	2180
Upper bushing weight: $m_{UB}.g$	lbs	2156	447	1570
Location of upper bushing center of gravity: H_{CM_UB}	in	87.6	34	85.2
Lower bushing weight: $m_{LB}.g$	lbs	554	293	510
Location of lower bushing center of gravity: H_{CM_LB}	in	59.2	28	39
Connection plate weight: $m_{CH}.g$	lbs	100	100	100
Weight per unit length	lb/in	11.07	4.89	8.15
Distance to the flange (half of the center pocket): H_F	in	11.5	13.4	11.5
Fixed frequency: f_{FIX}	Hz	9.36	21	9.35
As-installed frequency: f_{AI}	Hz	4.3	11.3	7.70
Material of insulator	-	Porcelain	Porcelain	Porcelain

The bushing is divided into upper and lower parts which are connected by a connection plate of thickness $2H_F$. The length of the upper part is equal to H_{UB} and the length of the lower part is equal to H_{LB}. The distance from the flange to the center of mass of the upper part of the bushing is equal to H_{CM_UB} and the distance from the flange to the center of mass of the lower part of the bushing is equal to H_{CM_LB}. The mass of the upper part of the bushing is equal to m_{UB}, the mass of the lower part of the bushing is equal to m_{LB} and the mass of the connection plate is equal to m_{CH}. Measurements of important parts of the bushing are shown in Figure 2.

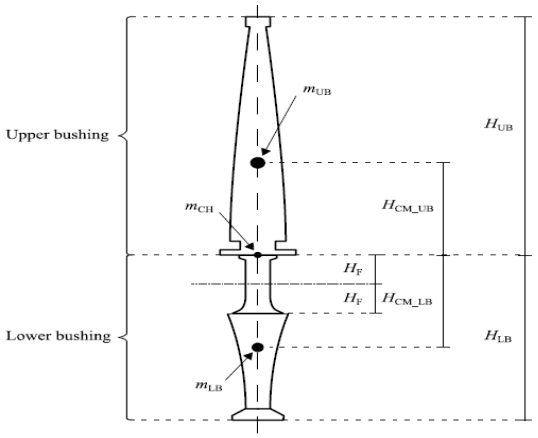

Fig. 2: Definition of dimensions of bushing

Each mode of vibration is damped at 3% of critical damping. This value of the damping ratio has been obtained using observations in previous field studies [44].

Calibration of the as-installed bushing model is done as follows. Given the geometry of a bushing and the values of the frequencies for the fixed and the as-installed conditions, f_{Fix} and f_{AI}, respectively, as in Table 1, these specifications are effective in constructing the analytical model of Figure 3 and are obtained according to the following steps [17]

a) the moment of inertia of the upper bushing I_{UB} is calculated:

$$f_{Fix} = \frac{1}{2\pi}\sqrt{\frac{3E_{UB}I_{UB}}{H_{CM\_UB}^3 m_{UB}}} \quad (2)$$

b) The vertical stiffness K_V is calculated from the following equation:

$$K_V = (2\pi f_V)^2.(m_{UB} + m_{CH} + m_{LB}) \quad (3)$$

c) A hypothetical value is considered for rotational stiffness K_θ, the fundamental frequency is calculated, and compared to the known value of the as-installed frequency f_{AI}.

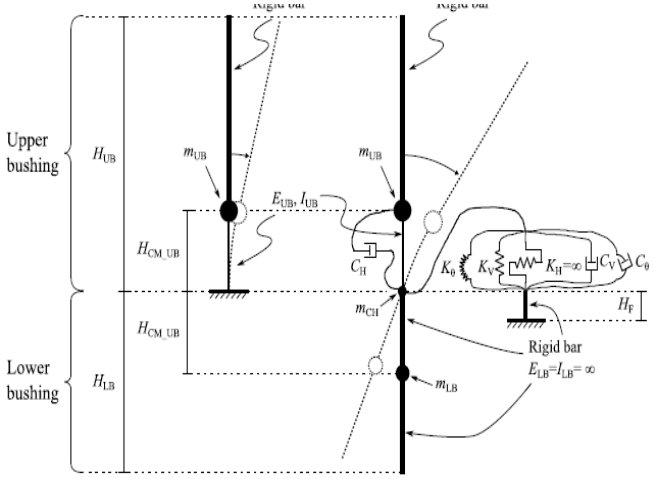

Fig. 3: Bushing models: (a) fixed condition; (b) as-installed condition

d) The vertical linear viscous damper constant C_V is calculated using the following equation:

$$C_V = 4\pi m_V.\beta_V.f_V \quad (4)$$

m_V is the effective mass in the vertical direction is calculated using Eq. (5):

$$m_V = m_{UB} + m_{CH} + m_{LB} \quad (5)$$

e) The circular frequency ω_θ at the joint of bushing and transformer body is calculated using Eq. (6):

$$\omega_\theta = \sqrt{K_\theta / I} \quad (6)$$

where I is the moment of inertia of the bushing. The rotational linear viscous damper constant C_θ is calculated using Eq. (7):

$$C_\theta = 2I.\beta_\theta.\omega_\theta \quad (7)$$

where β_θ is the damping ratio in a purely rotational mode:

$$C_\theta = \frac{K_\theta . \beta_\theta}{\pi . f_{AI}} \quad (8)$$

f) The horizontal linear damper constant C_H is calculated using Eq. (9):

$$C_H = 4\pi\beta_H m_{UB} f_{Fix} \quad (9)$$

where β_H is the damping ratio in a purely horizontal mode (0.03 is used).

3.2 Failure of transformers

Transformer failure can occur in a variety of ways. However, past studies have shown that bushing failure is the most crucial cause of transformer failure. The main failure modes of the bushing are shown in Figure 4 based on the observations of past earthquakes [42].

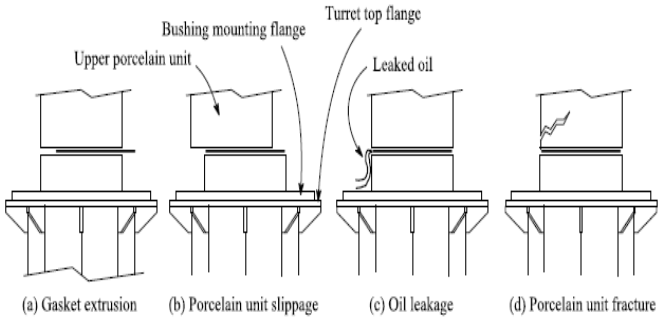

Fig. 4: Main failure modes of porcelain bushings

The calculation of the accelerations in the longitudinal and transverse bushing directions from values in the vertical and horizontal directions, and the acceleration limits, is demonstrated in Figure 5.

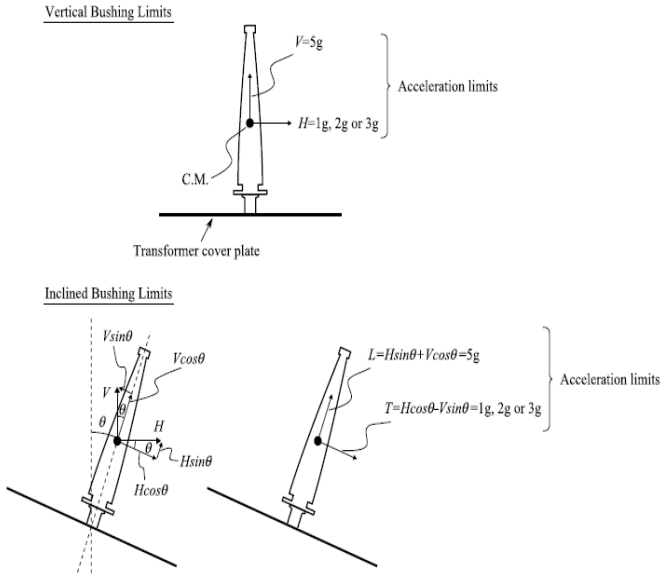

Fig. 5: Calculation of longitudinal and transverse bushing accelerations and limit states

3.3 Modeling of transformer

Figure 6 shows a two-dimensional model of a transformer. Each frame represents half of a transformer. Figure 6(a) shows the model of the transformer in the fixed base position, Figure 6(b) shows the transformer model in the horizontal isolation and Figure 6(c) shows the transformer model in the combined horizontal-vertical isolation system with or without rocking motion. The bushing is mounted vertically or at an angle of 20 degrees to the transformer. When the bushing is placed vertically on the transformer, θ is equal to zero and when it is placed sloping, θ is equal to 20 degrees.

In Figure 6(a), the length (or width) of the transformer is denoted by L_T and the distance from the ground to the center of mass of the transformer is denoted by H_T, in Figure 6(b), H_{TFP} is equal to the height of the triple FP isolator and H_C is equal to the height of the concrete slab and in Figure 6(c), H_{SD} is equal to the height of the spring-damper device.

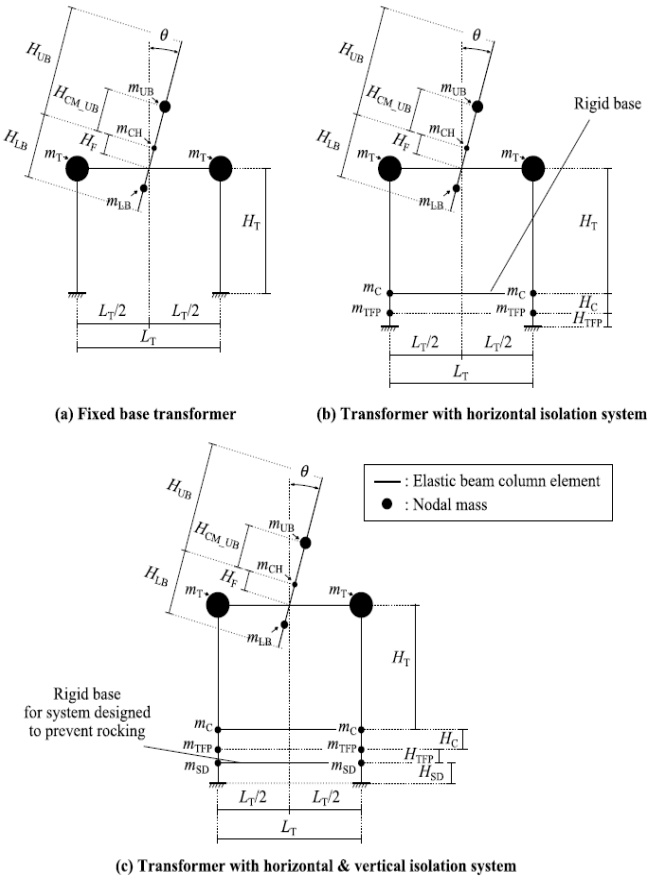

Fig. 6: Two-dimensional transformer models

Figure 7 shows the transformer isolated in the horizontal-only direction. Three bushings with frequencies of 4.3, 7.7, and 11.3 Hz are installed on this transformer, which covers a wide range of frequencies. and Figure 8 shows the longitudinal and transverse sections of a three-dimensional seismic isolated transformer with a rocking motion. This

system is termed three-dimensional seismic isolation, which describes its seismic performance.

Fig. 7: Seismically isolated transformer in Vancouver

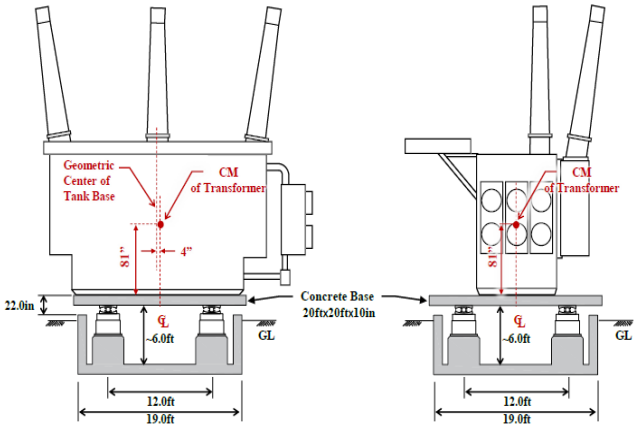

Fig. 8: longitudinal and transverse sections of a three-dimensional seismic isolated transformer with a rocking motion

4. Description of seismic isolation system and modeling in program OpenSEES

4.1 Triple friction pendulum isolators

A three-dimensional seismic isolation system includes triple FP isolators mounted on a vertical isolation system and provides horizontal isolation and the spring-damper device provides vertical isolation. The spring-damper device resists rotation and lateral displacement, which leads to the transfer of shear force and overturning moment by its upper support. Figure 9 shows the section and plan views of the example of the triple FP isolator considered in this study for transformers of weights 320, 420, and 520 kip.

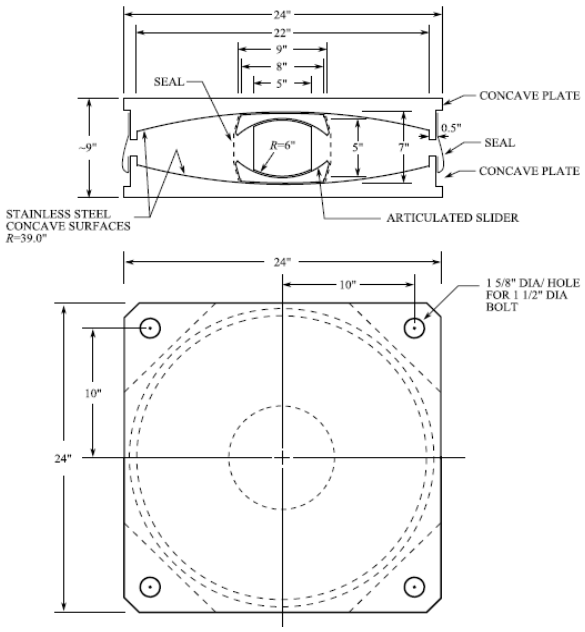

Fig. 9: Section and plan views of the smallest size triple FP bearing without inner restrainer

The behavior of the triple FP bearings has been defined in Fenz and Constantinou's 2008 work [45], and a more detailed description consisting of their ultimate characteristics is also presented in Sarlis and Constantinou's 2013 work [46]. Section 4.3 in this paper provides a model for the collapse of this bearing used in the program OpenSEES [47]. The model is a modification of the series model of Fenz and Constantinou [45] and consists of the effect of the inner restrainer based on the theory of Sarlis and Constantinou [46].

Table 2 shows the frictional characteristics of the triple FP isolators. Table values are calculated based on McVitty and Constantinou's 2015 work [48].

Note that the system property modification factors used for uncertainties in properties when only prototype test data are available (λ_{spec}) are set equal to unity because test data on all isolators are presumed available.

Table 2: Lower bound frictional characteristics of triple FP isolators

Load (kip)	$\mu_1 = \mu_4$	$\mu_2 = \mu_3$	Comments
80	0.130	0.095	For the 320 kip Transformer. Adjusted from test data at 110 kip load.
110	0.120	0.080	For the 420 kip transformer. Based on test data.
130	0.110	0.065	For the 520 kip transformer. Adjusted from test data at 110 kip load.
Test data are reported by Oikonomou et al. [8] For upper bound properties (excluding low-temperature effects), multiply values by 1.23.			

4.2 Description of the spring-damper device

The spring-damper device is designed for electrical transformers with total weight and consists of the triple FP isolators and any slab supporting the transformer on top of the isolators for the weight of 320, 420, and 520 kip.

The maximum static load per isolator is assumed to be 130 kip. The basic function of the vertical isolator unit is to support the weight and provide a frequency in the vertical direction of 2.0 Hz with a corresponding damping ratio of 0.50 critical when the total supported load is 420 kip. For the range of weights of 320 to 520 kip, the frequency and damping ratio will be 2.3 Hz and 0.56 when the weight is 320 kip and will be 1.8 Hz and 0.44, respectively, when the weight is 520 kip. The springs have linear elastic behavior, and the damper has linear viscous behavior. Table 3 presents the parameters of one of these devices. The device has a significant margin of safety (factor greater than 2) for the specified force and moment limits.

Table 3: Parameters of spring-damper device

Static load (per unit)	130 kip
Static deflection	3.0 inch
Stiffness per unit	44 kip/inch
Damping constant per unit (linear viscous damping)	3.4 kip-sec/inch
Dynamic deflection	±1.75 inch
Total deflection	4.75 inch
Stroke capacity	5.0 inch
Displacement capacity (from position of -3 inch static deflection; + is tension; - compression). Displacement limits change when the static load changes.	+3.0 inch
	-2.0 inch
Peak rotation allowed for a top plate concerning the bottom	0.1 degrees
Torsional rotation allowed	Zero

Figure 10 shows a schematic view of the device. In compression, the displacement capacity is used when it reaches the limit of 5.0-inch stroke, and then the device shows very high stiffness with really unlimited force capacity. The 5.0-inch limit is controlled by the design of the damper. Note that the springs have additional displacement capacity, which cannot be used. In tension, the device reaches the limit of 5.0-inch stroke, which is the displacement capacity of the damper (the springs have additional displacement capacity which cannot be utilized). After that, the device exhibits high stiffness until the ultimate force capacity of the damper in tension is reached. This force limit depends on the damper's design and is usually more than double the maximum damping force. For this device, the tensile limit is about 200 kip.

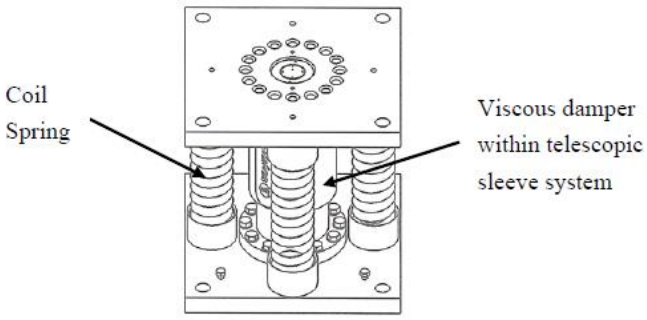

Fig. 10: Schematic of the spring-viscous damper device

Figure 11 shows the installation method with a free rocking motion. The bottom concave plate of the triple FP isolators can rotate according to a rotation angle β limited by the telescopic sleeve system. The angle β is low and restricted to 0.1 degrees. The rocking angle α is constrained by the ability of the spring-damper to move vertically. Based on the limitations listed in Table 3, the vertical displacement capacity is 3 inches downwards and 2 inches upwards (for a static load of 130 kip). The total angle of rotation $\alpha+\beta$ is thus less than about 1.1 degrees.

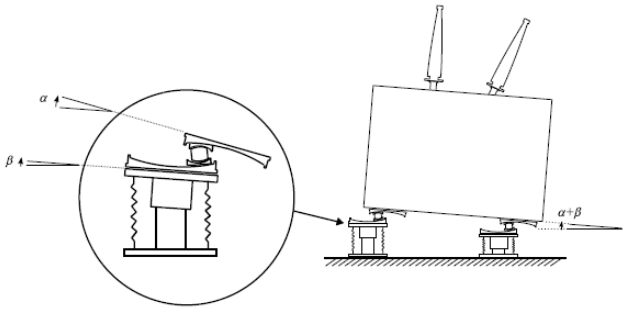

Fig. 11: Installation method that freely allows rocking

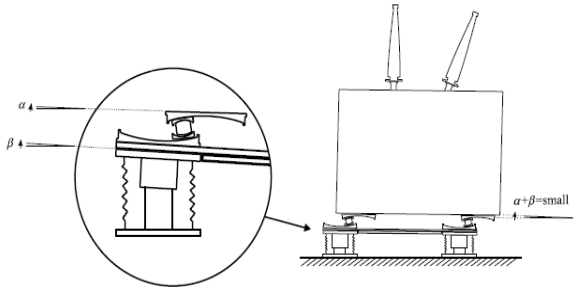

Fig. 12: Installation method that restrains rocking

Figure 12 shows the installation method in which the rocking motion is limited. When a stiff base is placed between the bottom FP concave plate and the top plate of the vertical spring-damper device, the rocking motion is limited and the rocking angle α is reduced to zero, so the total angle of rotation $\alpha+\beta$ is about 0.1 degrees. This method is effective

when the as-installed frequency of the bushing is close to the rocking frequency of the isolated transformer. In this case, the installation of a stiff base prevents the occurrence of the resonance phenomena and leads to a decrease in responses.

4.3 Model for simulating the ultimate behavior of the three-dimensional seismic isolation system in the OpenSEES software

4.3.1 Properties of transformer model

The body of the transformer is modeled by a rigid frame. The mass of the transformer body is displayed as two concentrated masses at the top of the frame, which is indicated by $2m_T$. The transformer frame is modeled by the elastic beam-column elements in OpenSEES software. The mass of the concrete slab is displayed at $2m_C$. The mass of the spring-damper device is shown with m_{SD} at the bearings and the mass of triple FP with m_{TFP} at the bearings is shown. All model specifications are shown in table 4.

Table 4: Model specifications of the transformer

Height of transformer: H_T	81 in
Length (width) of transformer: L_T	110 in
Height of concrete slab: H_C	6.0 in
Height of triple FP isolator: H_{TFP}	4.75 in
Height of spring-damper: H_{SD}	3.0 in
Anglea of inclination of bushing: θ	0 or 20 degrees
Lumped mass for transformer body: m_T	70, 95, 120 kip/g
Lumped mass for concrete slab: m_C	10 kip/g
Lumped mass for triple FP: m_{TFP}	0.7 kip/g
Lumped mass for spring damper: m_{SD}	0.5 kip/g
Total weight of isolated structure: $W_T + W_C = (m_T + m_C).g$, g = 386 inch/sec^2	320, 420, 520 kip

4.3.2. Model for simulating the ultimate behavior of triple friction pendulum bearings

The approach followed herein is to modify the series model in Fenz and Constantinou's 2008 work [45] to simulate the ultimate behavior of the triple FP as predicted by the theory presented in Sarlis and Constantinou's 2013 work [46]. The advantages of the modified series model are its simplicity and the ease of implementation in the OpenSEES software. The modified series model has three units, as shown in Figure 13. Each unit (FP1 to FP3) contains the following OpenSEES elements: (a) a single FP bearing element, (b) a MinMax material, and (c) an elastic-perfectly plastic gap material with two node-link element components.

The single FP bearing element can account for the effect of the varying axial load on the instantaneous stiffness and friction force. A simplified version of the model that neglects this interaction replaces the single FP element with axial, rotational, and horizontal springs in parallel, as shown in Figure 14. Note that this simplified model is computationally more stable.

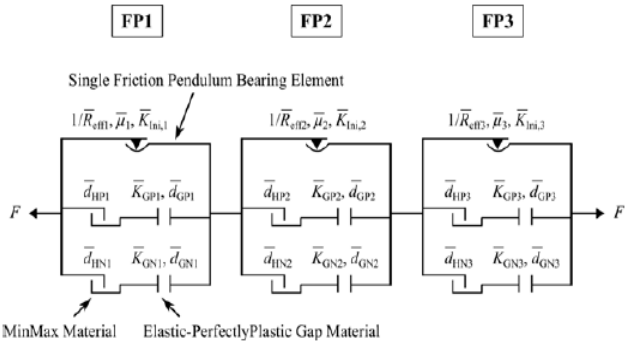

Fig. 13: Organization of elements of the modified series model in OpenSEES

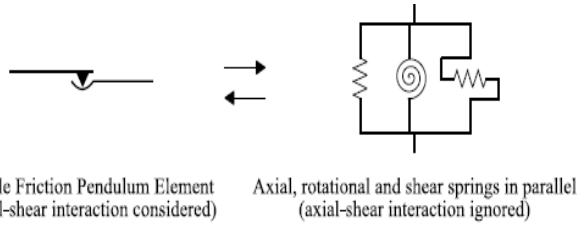

Fig. 14: Three springs in parallel element to replace single FP element

4.3.3 Model for simulating the ultimate behavior of the spring-damper unit

Three uniaxial elements are used to demonstrate spring behavior in the OpenSEES software [47]: i) elastic uniaxial material, ii) elastic-perfectly plastic material, and iii) elastic-perfectly plastic gap material. They are shown in Figure 15, and a force-displacement relation is for the entire element shown in Figure 16. Note that the springs are assumed to have a very low tensile stiffness when the displacement limit of 5.0 inches is exceeded (α times the actual stiffness where α =0.001).

The model shown in Figure 15 illustrates the behavior of the springs alone. Within the spring-damper assembly, the springs can only deform in compression up to a maximum of 5.0 inches from the unloaded position (as shown in Figure 15). In tension and without propounding the damper, the spring can deform as shown in Figure 15. The spring will be sustained by the damper, which has a stroke capacity of 5.0 inches. Thus, the springs cannot be stretched in tension as the force will then be transferred to the damper that has reached its displacement capacity and resists deformation with very high stiffness.

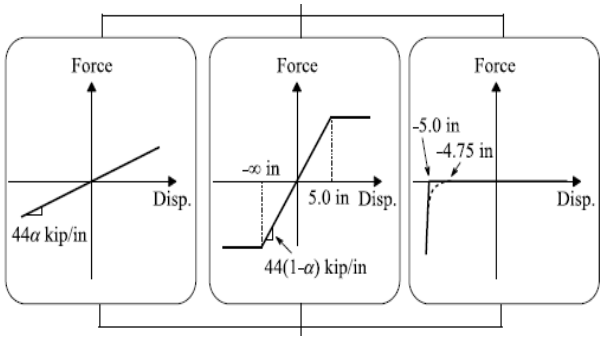

Fig. 15: Elements connected in parallel to represent the ultimate behavior of springs

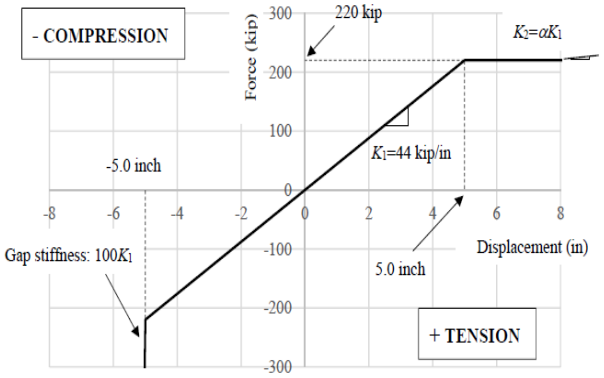

Fig. 16: Force-displacement relation produced by the spring element

The viscous damper is indicated in the OpenSEES software with a newly developed uniaxial material element called *ULTdamper*. The hysteretic rule for this element is presented in Figure 17. The viscous force is not shown for clarity. This force is simply linearly related to the velocity through the damping constant C (= 3.4 kip-s/inch). Other parameters for this model are shown in Figure 15, and values of parameters are demonstrated in Table 5. The tensile post-failure behavior of the device was described in a method that: (a) is physically meaningful and (b) is such that numerical instability in the analysis program is avoided. The failure behavior of the device was modeled so that when the device force reaches the ultimate value ("Ultimate F_{Tension}" in Figure 17), the force is not suddenly deleted but partly is gradually reduced at each time step by an amount equal to 10% of the value at the previous step. Note that when the damper element fails in tension and is removed from the spring-damper combined element, the element is still functional but with only the spring being efficient.

Table 5: Parameters for viscous damper

D_{Capacity}P	0.0 inch
D_{Capacity}N	-5.0inch
Ultimate $F_{\text{Compression}}$	unlimited
Ultimate F_{Tension}	200 kip

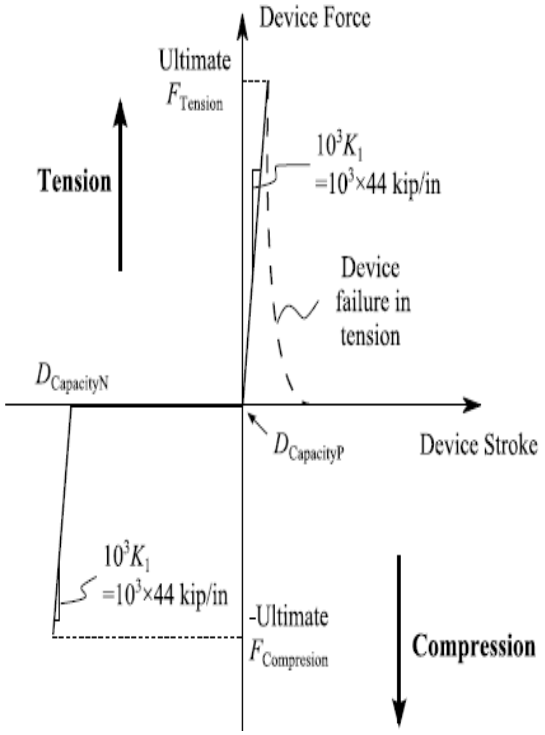

Fig. 17: Ultimate behavior of viscous damper element (viscous force not depicted)

Representative force-displacement relations produced by the damper element are shown in Figure 18. Three different force-displacement hysteresis loops are shown in Figure 15. All loops were generated by imposing motion from a defined static position and amplitude of 2.3 inches at a frequency of 2 Hz. The second two loops result either in failure in tension or reaching the bottom of the damper, thus producing very high compressive force. It is necessary to mention that when a triple FP isolator is located on top of the spring-damper unit, failure in tension is not feasible as uplift will happen at the isolator before importing tension into the damper.

5. Selection and scaling of ground motions To perform incremental dynamic analysis (IDA)

Failure resistance evaluation requires carrying out IDA, which is used to assess the probability of failure for a specific set of motions per FEMA P695 procedures. While the procedures in FEMA P695 only consist of the horizontal components of ground motions, the analysis utilized in this work needs that vertical component are also included. This is essential in evaluating the performance of the three-dimensional isolation system.

Far-field horizontal ground motions were selected from the suite of motions utilized in FEMA P695, and the corresponding vertical components were taken from the PEER website (PEER, accessed 9 Nov. 2015) [49].

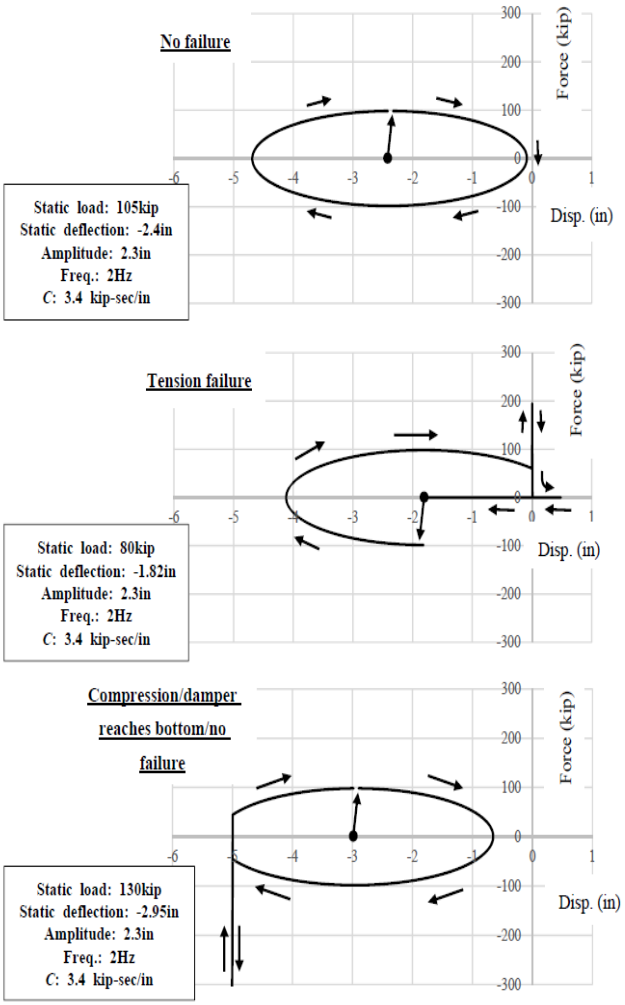

Fig. 18: Force-Displacement loops produced by damper element

Table 6 shows the information on ground motions utilized in this study. The magnitude of the motions is in the range of 6.5 to 7.6, with an average magnitude of 7.0. Figures 19 and 20 show the 5%-damped acceleration response spectra for the horizontal and vertical ground motions, respectively.

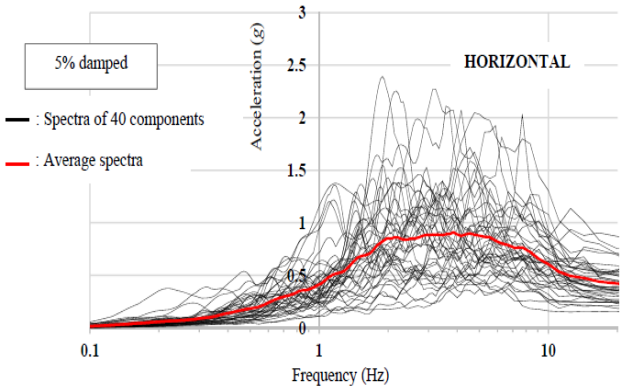

Fig. 19: Horizontal acceleration response spectra of selected 20 ground motions (total of 40 components)

Table 6: Far-field ground motions used in dynamic analysis

Earthquake name	Recording Station Name	Values shown are in two horizontal directions, then vertical; unit g
		PGA
Northridge	Beverly Hills - Mulhol	0.42, 0.52, 0.32
Northridge	Canyon Country WLC	0.41, 0.48, 0.30
Duzce, Turkey	Bolu	0.73, 0.82, 0.20
Hector Mine	Hector	0.27, 0.34, 0.15
Imperial Valley	Delta	0.24, 0/35, 0.14
Imperial Valley	El Centro Array #11	0.36, 0.38, 0.38
Kobe, Japan	Nishi-Akashi	0.51, 0.50, 0.39
Kobe, Japan	Shin-Osaka	0.24, 0.21, 0.06
Kocaeli, Turkey	Duzce	0.31, 0.36, 0.21
Kocaeli, Turkey	Arcelik	0.22, 0.15, 00.8
Landers	Yarmo Fire Station	0.24, 0.15, 0 14
Landers	Coolwater	0.28, 0.42, 0.18
Loma Prieta	Capitola	0.53, 0.44, 0.56
Loma Prieta	Gilroy Array #3	0.56, 0.34, 0.34
Manjil, Iran	Abbar	0.51, 0.50, 0.54
Superstition Hills	El Centro Imp. Co	0.36, 0.26, 0.13
Chi-Chi, Taiwan	CHY101	0.35, 0.44, 0.17
Chi-Chi Taiwan	TCU045	0.47, 0.51, 0.36
San Fernando	LA - Hollywood Stor	0.21, 0.17, 0.16
Friuli- Italy	Tolmezzo	0.35, 0.31, 0.28

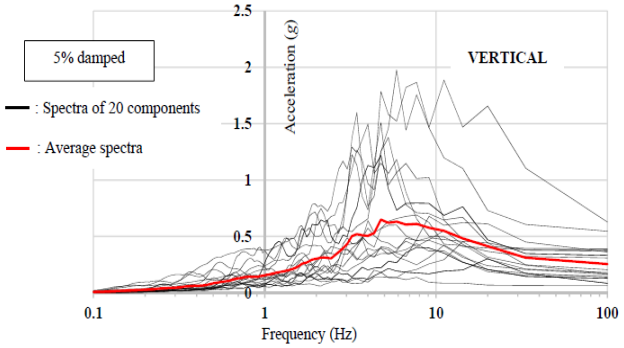

Fig. 20: Vertical acceleration response spectra of selected 20 ground motions (total of 20 components)

Figure 21 compares the average spectra of the selected motions when scaled to a PGA of 0.5g in the horizontal direction, and a PGA of 0.4g in the vertical direction to the IEEE high required response spectra (Figure 1).

It may be seen that the horizontal average spectrum falls below the IEEE spectrum but has a wide frequency range consistent with the IEEE spectrum, whereas the vertical average spectrum deviates from the IEEE vertical spectrum. The average vertical spectrum correctly displays a narrower range and higher values of frequencies than the horizontal spectrum, which is not appropriately displayed in the IEEE spectrum. Figure 18 also consists of the average spectra of the scaled motions; thus, the PGA is 0.6g rather than 0.5g (horizontal PGA is 0.6g, vertical PGA is 0.48g). The

horizontal scaled motions now better show the IEEE spectrum for frequencies larger than about 2 Hz, so the use of the results of the fragility analyses in this paper for a PGA of 0.6g may be a suitable demonstrator of behavior for the IEEE PGA 0.5g seismic motions.

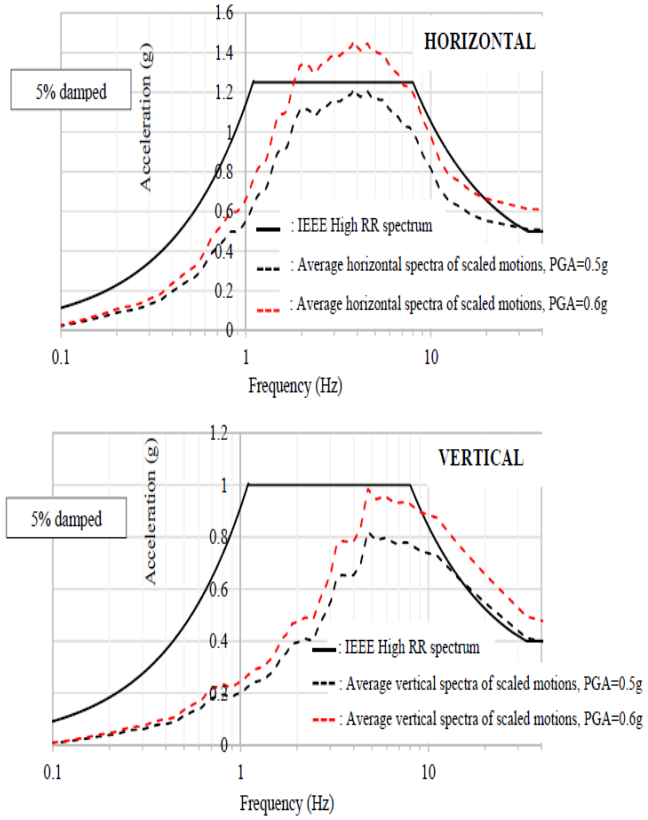

Fig. 21: Comparison of horizontal and vertical average spectra to IEEE high required response spectra

To perform IDA, the selected ground motions need to be progressively increased in intensity. The approach conformed is to increase the acceleration of the horizontal component of each pair of horizontal-vertical motions while keeping the vertical to horizontal peak acceleration ratio the same as in the original, as-recorded motion. The approach to scaling the horizontal component is similar to the approach to scaling the Sa component of FEMA P695.

The scaled motions are applied to repeatedly analyze the transformer model by increasing the intensity; thus, the peak acceleration of the horizontal component of each pair increases by increments of 0.05*g* until there is the failure of either the bushings or the isolators. The vertical component of each pair of ground motions is increased by an amount different than 0.05g so that the final scaled pair maintains the peak vertical to peak horizontal acceleration ratio as in the originally recorded ground motion.

6. Evaluation of Near-Fault Pulse-Like Excitations

Towns close to the active fault zone are more susceptible to the consequences of seismic risks. In such an area, the seismic risk can be significantly increased because of the proximity of the built environment to the hazard source. The characteristics of near-field earthquakes can greatly affect the seismic performance of buildings. The most important ones are fling step and forward directivity. In many cases, the latter results in a ground motion similar to pulses in sites placed in the direction of seismic wave propagation. This type of signal contains a velocity pulse, meaning that a higher energy level is released in a short amount of time. This causes more severe structural damage than non-impulsive recorded signals, which highlights the need to put more effort into studying the characteristics of the pulsed signal[50].

Numerous studies on the pulse-like excitations have been performed by Somerville et al. [51]. They Suggested a modified method to consider the effects of rupture directivity. Huang et al. [52] investigated the maximum seismic spectral demand in the near-fault region. Almufti et al. [53] Showed the effect of velocity pulse on the design of structures.

Some of the considered sites qualify for classification as being in the proximity of active faults with pulse-like characteristics, with the closest fault being within 1km to 4km. For these locations, the fragility analysis results need to be reassessed by conducting the nonlinear dynamic analysis using motions with near-fault characteristics. FEMA (2009) provided a set of such motions, including 28 records of bidirectional components (56 individual horizontal components) for use in these cases. Table 5 presents a subset of 13 of these records for which the vertical ground motion component was available.

Figures 22 and 23 present the 5%-damped acceleration response spectra for the horizontal and vertical ground motions, respectively. The horizontal spectra consist of the 50 spectra of fault normal and fault parallel components, and the vertical spectra consist of the 25 spectra of the vertical components [21]. The average spectra are also shown for each direction. All of the records (see Table 7) do contain such pulses.

Nonlinear dynamic analysis was performed using the near-fault motions for the three cases of bushing as-installed frequencies (4.3, 7.7, and 11.3 Hz) of the 320 and 420 and 520 kip transformers without and with isolators of displacement capacity $D_{Capacity}$ = 17.7 (in), 27.7 (in), 31.3 (in).

Table 7: Near-Fault pulse-like ground motions used in dynamic analysis

Earthquake			Recording Station	Values shown are in two horizontal directions, then vertical; units g, in/sec	
M	Year	Name	Name	PGA	PGV
Pulse Records Subset					
6.5	1979	Imperial Valley-06	El Centro Array #6	0.44, 0.40, 1.89	44.0, 25.5, 25.0
6.5	1979	Imperial Valley-06	El Centro Array #7	0.46, 034, 0.58	42.8, 17.5, 10.7
6.9	1980	Irpinia, Italy - 01	Sturno	0.23 0.31 0.23	163, 17.9, 9.5
6.9	1989	Loma Prieta	Sarato - Aloha	0.36, 0.38, 0.40	21 .9, 17.0, 11.0
6.7	1992	Erzican, Turk	Erzincan	0.49, 0.42, 0.23	37.4, 17.8, 6.5
7	1992	Cape Mendocino	Petrolia	0.61, 0.63, 0.17	32.2, 23.8, 8.0
7.3	1992	Landers	Lucerne	0.71, 0.79, 0.82	55.1, 20.8, 16.2
6.7	1994	Northrid -01	Rinaldi Receivin Sta	0.87, 0.42, 0.96	65.7, 24.6, 16.6
6.7	1994	Northridge-O I	Sylmar - Olive View	0.73, 0.60, 0.54	48.3, 21.4, 7.3
7.5	1999	Kocaeli, Turk	Ian it	0.15, 0.22, 0.14	8.9, 11.7, 4.9
7.6	1999	Chi-Chi, Taiwan	TCU065	0.82, 0.59, 0.26	50.2, 31.6, 27.3
7.6	1999	Chi-Chi, Taiwan	TCU102	0.29, 0.1 7, 0.18	41 .9, 30.5, 26.9
7.1	1999	Duzce, Turk	Duzce	0.36, 0.52, 0.35	24.5, 31.2, 7.9

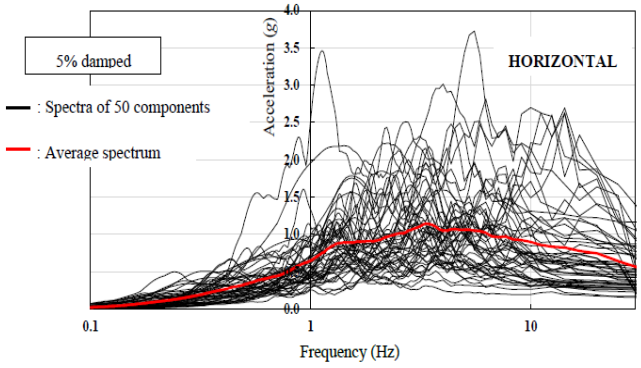

Fig. 22: Horizontal acceleration response spectra of selected 25 near-field ground motions (total of 50 components)

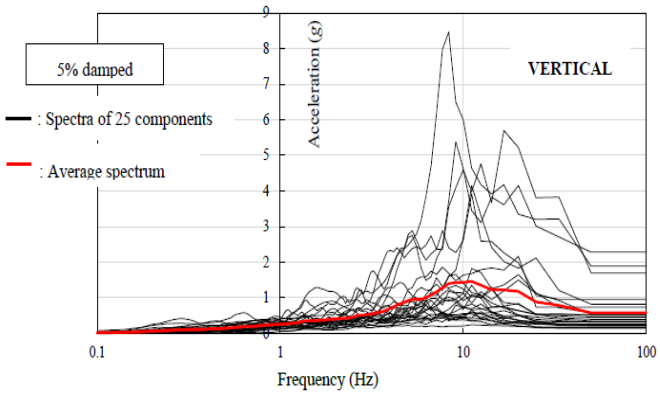

Fig. 23: Vertical acceleration response spectra of selected 25 near-field ground motions (total of 25 components)

To investigate the effects of near-fault motions with pulse-like characteristics, the results of the analyses were evaluated. For example, the history of the acceleration at the center of mass (CM) of the bushing in the transverse direction in the Imperial valley Earthquake-06 (El Centro Array#6 record) is shown in Figure 24 in the fixed base position, horizontal isolation, and three-dimensional isolation system with rocking, respectively. The results show that only horizontal isolation reduces the maximum horizontal acceleration of the CM of the bushing by about 30% relative to the fixed base position. In contrast, a three-dimensional isolation system with rocking motion has a much more significant effect on reducing the acceleration of the CM of the bushing, so that it reduces the maximum horizontal acceleration of the CM of the bushing by about 75% compared to the fixed base position. Hence, using a three-dimensional isolation system in near-fault motions with pulse-like characteristics is very cost-effective and reduces the failure probability of the transformer. Figure 24 shows the acceleration values in different models.

In the following, to evaluate the seismic performance of the three-dimensional isolation system in the near-fault excitation with pulse-like characteristics, the horizontal displacement of the triple FP isolator and the vertical displacement of the spring-damper unit were measured. The results show a sharp increase in horizontal displacement of

the triple FP and vertical displacement of the spring-damper unit compared to the far-field motions. The maximum horizontal displacement of the triple FP isolator has reached about 15.0 inches, which has increased more than three times compared to far-field motions. Figure 25 compares the response history of horizontal displacement of triple friction pendulum isolator in the far-field ground motion (Northridge Earthquake, Beverly Hills-Mulhol record) with the near-fault pulse-like ground motion (Imperial valley Earthquake-06, El Centro Array#6 record).

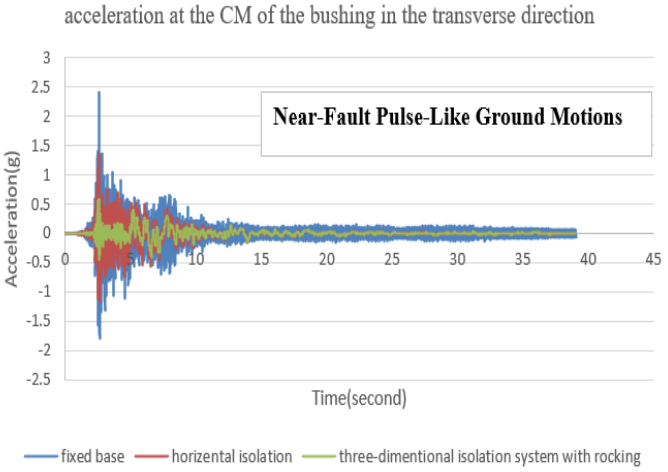

Fig. 24: Acceleration at the CM of the bushing in the transverse direction in the Imperial valley Earthquake-06 (El Centro Array#6 record)

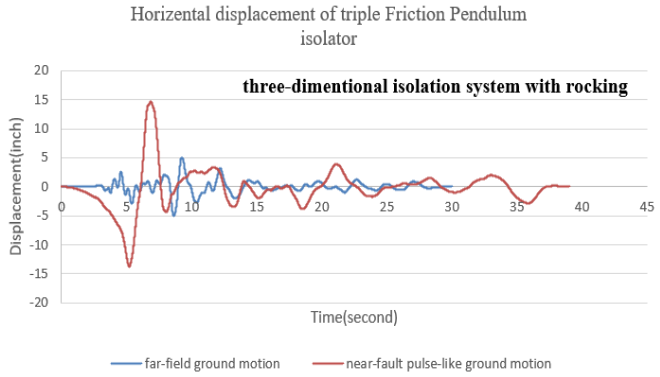

Fig. 25: Comparison of horizontal displacement of triple FP isolator in the far-field ground motion with the near-fault pulse-like excitation

Also, the dynamic vertical displacement of the spring-damper unit isolator has reached about 2.3 inches, which has more than doubled compared to far-field motions, so in the near-fault motions with pulse-like characteristics, the horizontal and vertical displacement of the three-dimensional seismic isolation system increases sharply, and this leads to an increase in the horizontal displacement capacity of the triple FP isolator and the vertical dynamic displacement of the spring-damper unit. Hence, in near-fault motions with pulse-like characteristics, the use of three-dimensional isolation improves the seismic performance of the transformer and significantly reduces the failure probability of the transformer.

7. Fragility analysis results

Fragility analysis has been performed, and results are shown in terms of curves of the probability of failure versus PGA for the cases in Table 8.

Table 8: Analyzed cases of non-isolated and isolated transformers

Case	Parameters
Transformer (by weight in kip)	320; 420; 520
Bushing (by No. and frequency per Table 1	3 (f=4.3 Hz); 6 (f=11.3 Hz); 8 (f=7.7 Hz)
Bushing Inclination (degrees)	0; 20
Bushing acceleration limit (g)	1 or 2g for the transverse direction and 5g for the longitudinal direction
Isolation system type	Non-isolated; isolated in the horizontal direction; three-dimensional isolation with rocking
Horizontal isolation system ultimate displacement capacity (inch)	17.7; 27.7; 31.3(without inner restrainer)
Vertical isolation system (vertical stiffness and damping constant per isolator, stroke)	K=44 kip/in, C=3.4 kip-s/in, Stroke 5 in

Failure is specified when any of the following criteria is to happen, whichever occurs first [18]:

1) The acceleration at the CM of the bushing in the longitudinal bushing direction exceeds 5g, or

2) The acceleration at the CM of the bushing in the transverse direction exceeds 1g or 2g (two different cases), or

3) The triple FP isolator horizontal displacement exceeds the ultimate capacity limit of 17.7, 27.7, and 31.3 inches (three different cases), or

4) The net uplift FP isolator displacement exceeds 2.0 inches, or

5) The analysis terminates due to numerical instability problems.

7.1 Fragility data for far-field motions

Incremental dynamic analyses have been performed using the far-field motions for transformers and bushings listed in Table 4 and the values of PGA_F a and β (dispersion factor) are shown in Table 9.

Table 9: Fragility data of the analyzed transformers for far-field motions

Transformer Weight (kip)	Bushing Freq.(Hz)	Isolator Displ. Capacity (inch)	Bushing Accel. Limit (g)	Non Isolated		Horizontal Isolation Only		three-dimensional isolation system with rocking	
				PGA_F(g)	β	PGA_F(g)	β	PGA_F(g)	β
320	7.7	17.7	2	0.76	0.36	1.01	0.31	1.31	0.34
			1	0.38	0.36	0.77	0.38	1.03	0.30
420	4.3	17.7	2	0.93	0.27	0.94	0.30	1.23	0.36
			1	0.47	0.27	0.92	0.30	0.89	0.36
	7.7	17.7	2	0.76	0.36	0.96	0.30	1.29	0.36
			1	0.38	0.36	0.78	0.36	1.02	0.31
		27.7	2	0.76	0.36	1.13	0.32	1.66	0.35
			1	0.38	0.36	0.86	0.37	1.46	0.33
		31.3	2	0.76	0.36	1.25	0.36	1.96	0.38
			1	0.38	0.36	0.84	0.39	1.58	0.36
	11.3	17.7	2	1.37	0.28	0.92	0.31	1.38	0.37
			1	0.68	0.28	0.77	0.32	1.28	0.35
		27.7	2	1.37	0.28	1.05	0.34	1.74	0.36
			1	0.68	0.28	0.82	0.34	1.58	0.34
520	7.7	17.7	2	0.76	0.36	0.94	0.32	1.09	0.34
			1	0.38	0.36	0.78	0.36	1.01	0.32

Figures 26 and 27 present fragility curves for the 420 kip transformer with the 7.7 Hz (No. 8) bushing inclined at 20 degrees and with the triple FP isolators having 17.7-inch displacement capacity in the lower bound friction case and without an inner restrainer for far-field motions and transverse acceleration limit equal to 1g and 2g, respectively.

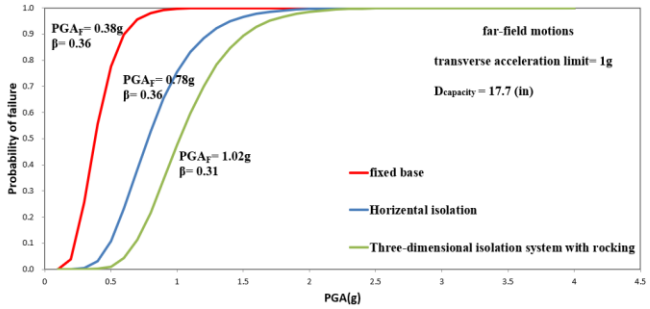

Fig. 26: Fragility curves for 420 kip transformer with 7.7 Hz bushing (No. 8) inclined at 20 degrees, isolator ultimate displacement capacity of 17.7 inches for far-field motions, transverse acceleration limit = 1g

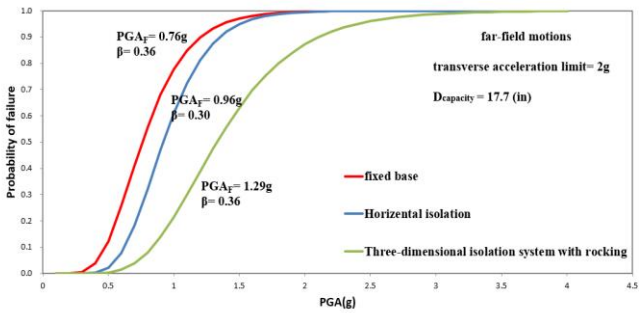

Fig. 27: Fragility curves for 420 kip transformer with 7.7 Hz bushing (No. 8) inclined at 20 degrees, isolator ultimate displacement capacity of 17.7 inches for far-field motions, transverse acceleration limit = 2g

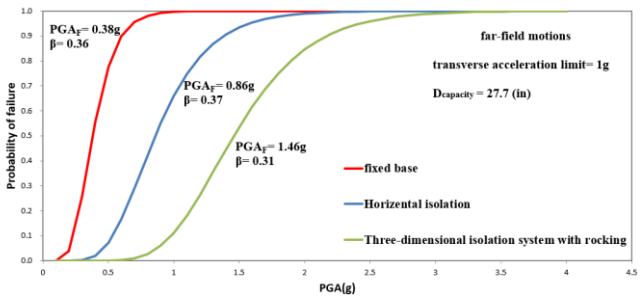

Fig. 28: Fragility curves for 420 kip transformer with 7.7 Hz bushing (No. 8) inclined at 20 degrees, isolator ultimate displacement capacity of 27.7 inches for far-field motions, transverse acceleration limit = 1g

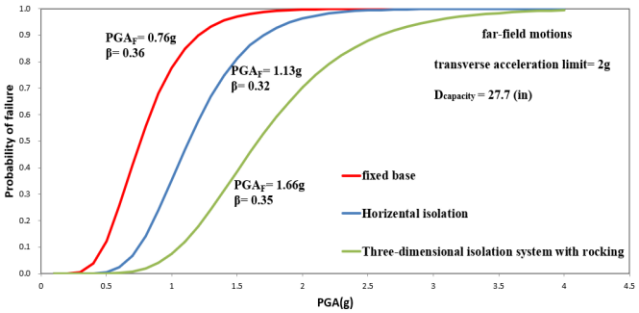

Fig. 29: Fragility curves for 420 kip transformer with 7.7 Hz bushing (No. 8) inclined at 20 degrees, isolator ultimate displacement capacity of 27.7 inches for far-field motions, transverse acceleration limit = 2g

7.1.1 The effect of increasing the displacement capacity of triple FP

To investigate the effect of increasing the displacement capacity of the triple FP isolator in PGA_F values, incremental dynamic analyses have been performed for the triple FP

isolator with a capacity of 27.7 inches. The corresponding fragility curves are displayed for transverse acceleration limits equal to 1g and 2g in Figures 28 and 29, respectively. The results show that increasing the displacement capacity of the triple FP isolator has a significant effect on increasing the PGA_F values because the horizontal isolation system reaches the failure limit later, and thus the seismic performance of the isolation system improves.

7.1.2 The effect of the vertically placed bushing

Figure 30 presents fragility curves for the same systems as those for which fragility curves are shown in Figure 26 but for the bushings that are vertically placed instead of inclined at 20 degrees. There are slight differences between the two cases, apparently due to the small inclination angle, except for the horizontal-only isolated transformer when the transverse acceleration limit is 1g. Then there is a noticeable reduction in the probability of failure when the bushing is vertical. This is likely due to a small contribution of the vertical component of the earthquake in magnifying the transverse acceleration of inclined bushings. This is more pronounced in the horizontal-only isolated transformer due to the lack of vertical isolation that mitigates the vertical earthquake effect.

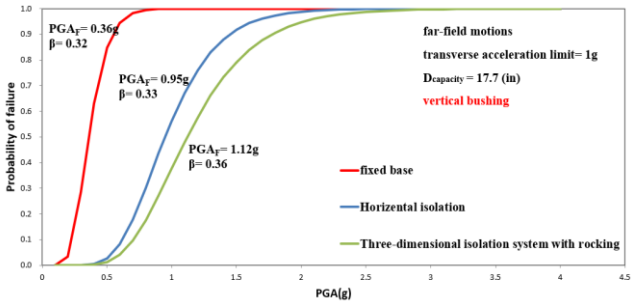

Fig. 30: Fragility curves for 420 kip transformer with 7.7 Hz bushing (No. 8), vertically placed bushing, isolator ultimate displacement capacity of 17.7 inches for far-field motions, transverse acceleration limit = 1g

7.2 Fragility data for pulse-like excitations

Incremental dynamic analyzes have been performed using the near-field motions for transformers and bushings listed in Table 5 and the values of PGA_F a and β (dispersion factor) are shown in Table 10.

Table 10: Fragility data of analyzed transformers for near-fault pulse-like excitation

Transformer Weight (kip)	Bushing Freq. (Hz)	Isolator Displ. Capacity (inch)	Bushing Accel. Limit (g)	Non Isolated		Horizontal Isolation Only		three-dimensional isolation system with rocking	
				PGA_F(g)	β	PGA_F(g)	β	PGA_F(g)	β
320	7.7	17.7	2	0.50	0.40	0.76	0.32	1.22	0.38
			1	0.25	0.40	0.58	0.38	0.95	0.33
420	4.3	17.7	2	0.61	0.30	0.76	0.31	1.14	0.40
			1	0.31	0.30	0.69	0.30	0.83	0.40
	7.7	17.7	2	0.50	0.40	0.72	0.31	1.20	0.40
			1	0.25	0.40	0.58	0.36	0.95	0.34
		27.7	2	0.50	0.40	0.85	0.32	1.55	0.39
			1	0.25	0.40	0.65	0.37	1.36	0.36
		31.3	2	0.50	0.40	0.94	0.36	1.82	0.41
			1	0.25	0.40	0.63	0.40	1.47	0.40
	11.3	17.7	2	0.90	0.31	0.69	0.32	1.28	0.40
			1	0.45	0.31	0.58	0.32	1.19	0.39
		27.7	2	0.90	0.31	0.78	0.34	1.62	0.40
			1	0.45	0.31	0.61	0.35	1.47	0.38
520	7.7	17.7	2	0.50	0.40	0.71	0.32	1.02	0.38
			1	0.25	0.38	0.58	0.36	0.94	0.35

Figures 31 and 32 present fragility curves for the 420 kip transformer with the 7.7 Hz (No. 8) bushing inclined at 20 degrees and with the triple FP isolators having 17.7-inch displacement capacity in the lower bound friction case and without an inner restrainer for near-fault pulse-like excitation and transverse acceleration limits equal to 1g and 2g, respectively.

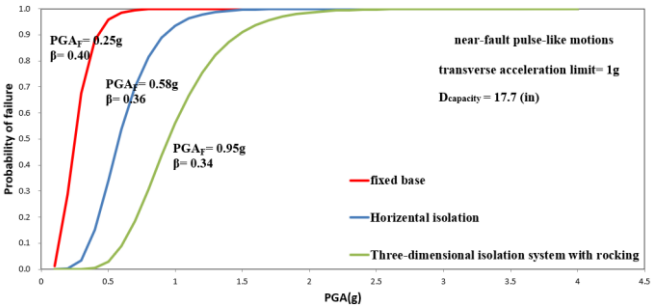

Fig. 31: Fragility curves for 420 kip transformer with 7.7 Hz bushing (No. 8) inclined at 20 degrees, isolator ultimate displacement capacity of 17.7 inches for near-fault pulse-like motions, transverse acceleration limit = 1g

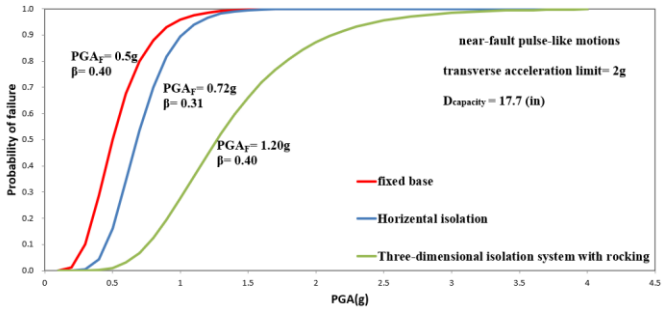

Fig. 32: Fragility curves for 420 kip transformer with 7.7 Hz bushing (No. 8) inclined at 20 degrees, isolator ultimate displacement capacity of 17.7 inches for near-fault pulse-like motions, transverse acceleration limit = 2g

7.2.1 The effect of near-fault pulse-like motions

A comparison of the fragility curves of far-field motions and near-fault pulse-like motions clearly shows that the values of PGA_F in the pulse-like excitation decrease sharply, and therefore the failure of the transformer and isolation system occurs sooner and leads to a decrease in PGA_F values. Thus, under pulse-like excitations, it is necessary to increase the displacement capacity of the triple FP isolator. Incremental dynamic analysis has been performed using a three-dimensional seismic isolation system with a displacement capacity of triple FP equal to 27.7 inches, and the corresponding fragility curves are shown in Figures 33 and 34.

Increasing the displacement capacity of the triple FP under pulse-like excitations will have a significant effect on improving the seismic performance of the three-dimensional seismic isolation system with rocking.

As an important result, the fragility curves in Figures 33 and 34 show that the use of a three-dimensional isolation system with rocking increases the PGA_F values by more than 80% compared to the horizontal isolation only, so, when the transverse acceleration limit of the bushing is equal to 2g, using three-dimensional isolation system with a more horizontal capacity of triple FP, is very effective in improving the seismic performance of the isolated transformer and reduces the probability of failure.

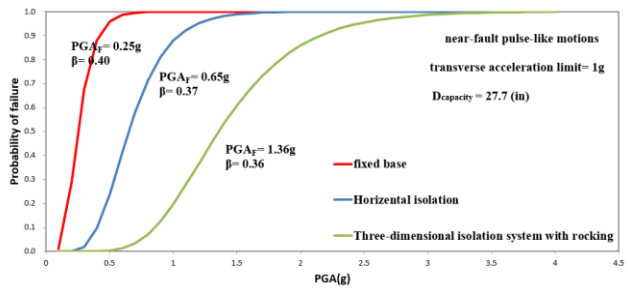

Fig. 33: Fragility curves for 420 kip transformer with 7.7 Hz bushing (No. 8) inclined at 20 degrees, isolator ultimate displacement capacity of 27.7 inches for near-fault pulse-like motions, transverse acceleration limit = 1g

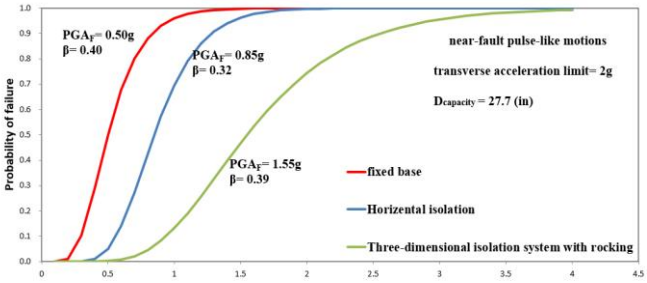

Fig. 34: Fragility curves for 420 kip transformer with 7.7 Hz bushing (No. 8) inclined at 20 degrees, isolator ultimate displacement capacity of 27.7 inches for near-fault pulse-like motions, transverse acceleration limit = 2g

7.2.2 The effect of different frequencies of the as-installed bushing

Also, the fragility data were examined to investigate the effect of different frequencies of the as-installed bushing on the mean value (PGAF) [54]. The results show that with increasing the total weight of the bushing, which leads to a decrease in the frequency of the as-installed bushing, the mean values (PGA_F) decrease, so the probability of transformer failure increases. Figure 35 shows the fragility curves for the 420 kip transformer with 4.3, 7.7, and 11.3 Hz bushing (No. 8) inclined at 20 degrees for a three-dimensional seismic isolation system with rocking.

Hence, one of the most critical factors in the probability of failure of the transformer is the frequency of the as-installed bushing. Note that according to previous studies, the rocking frequency of the three-dimensional isolated transformer system is equal to 2.7 Hz [55]; thus, the proximity of this frequency to the frequency of the as-installed bushing leads to amplification of response, so, the system with a stiff base is preferred as it can be designed to prevent or reduce rocking and avoid or reduce resonance (see Figure 12).

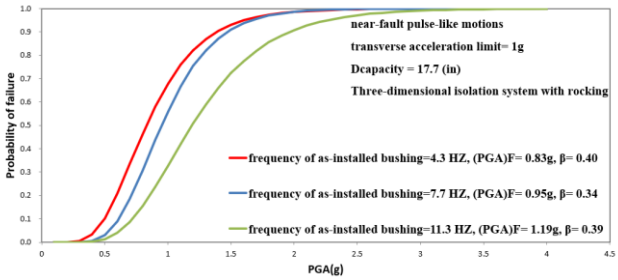

Fig. 35: Fragility curves for 420 kip transformer with 4.3, 7.7, 11.3 Hz bushing (No. 8) inclined at 20 degrees, isolator ultimate displacement capacity of 17.7 inches for near-fault pulse-like motions, transverse acceleration limit = 1g

7.2.3 The effect of the weight of different transformers

In the following, to investigate the effect of the weight of different transformers on the probability of failure, transformers weighing 320, 420, and 520 kip with an isolator

ultimate displacement capacity of 17.7 inches were tested. Examination of fragility data shows that when the bushing limit state is considered to be equal to 1g, increasing the bushing weight has no significant effect on changing the mean values(PGA_F), but when the bushing limit state is considered equal to 2g, increasing the weight of the transformer from 420 kip to 520 kip, reduces the mean values (PGA_F) by a maximum of 18% and therefore increases the probability of failure. Figure 36 shows the fragility curves for transformers of different weights for a three-dimensional isolation system with rocking.

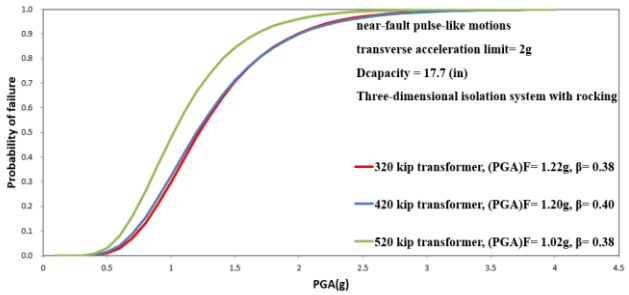

Fig. 36: Fragility curves for 320, 420, and 520 kip transformer with 7.7 Hz bushing (No. 8) inclined at 20 degrees, isolator ultimate displacement capacity of 17.7 inches for near-fault pulse-like motions, transverse acceleration limit = 2g

8. Summary and Conclusions

This paper provides numerical modeling of isolated transformers and compares the seismic performance of three-dimensional isolated transformers with isolated horizontal-only isolated transformers or non-isolated transformers. The horizontal isolation includes triple FP isolators and the vertical isolation includes a spring-damper device. Modeling of bushings and transformers and seismic isolation systems in horizontal and vertical directions was performed in OpenSEES software for different bushings and transformers in isolation systems with different displacement capacities. Modeling of a three-dimensional seismic isolation system is done by two methods. In the first method, the rocking motion is free and the total rotation angle is 1.1 degrees. in the second method, the rocking motion is limited and the total rotation angle is 0.1 degrees.
Seismic performance is assessed by calculating the probability of failure as a function of peak ground acceleration. The limit states used to evaluate the seismic performance of isolated transformers include the (a) acceleration limit of the longitudinal and transverse directions of the bushing, (b) the displacement capacity of the horizontal isolation system, (c) the uplift capacity of triple FP isolators and (d) the impact capacity of the vertical isolation system. Any of the above-limit situations that occur sooner is considered a measure of failure. Bushing acceleration limits were selected to evaluate transformer failure using field observations and empirical fragility data in past earthquakes. Due to the lack of investigation of the effect of near-fault ground motions with pulse-like characteristics on the seismic performance of isolated transformers in previous studies, incremental dynamic analysis was performed in far-field and near-field ground motions. The results are as follows:
1) Seismic isolation, whether horizontal-only or three-dimensional seismic isolation system, significantly reduces the probability of failure compared to non-isolated transformers.
2) Given the occurrence of an earthquake representative of the IEEE high required response spectra, defined herein to have a PGA = 0.6g, the non-isolated transformers have an unacceptably high probability of failure. In addition, the horizontal-only isolated transformers have a lower but still high probability of failure.
3) The performance evaluation procedures described in this paper may be used to decide on the benefits offered by the seismic protective system depending on the limits of the protected equipment, location of the equipment (value of PGA or near-fault ground motions), and configuration and properties of the seismic protective system.
Based on the new results in this paper, three-dimensional seismic isolation systems offer the lowest probabilities of failure for all cases of transformer and isolation system parameters and all considered ground motions. Horizontal-only isolation offers insignificant advantages over non-isolation when the bushing transverse acceleration limit is 2g. However, horizontal-only isolation offers important advantages over non-isolation when the bushing transverse acceleration limit is 1g.
Moreover, the paper presents sample results for near-fault pulse-like ground motions. To investigate the effects of near-fault motions with pulse-like characteristics, the results of the analyses were evaluated. The results show a sharp increase in horizontal displacement of the triple FP and vertical displacement of the spring-damper unit compared to the far-field motions. The maximum horizontal displacement of the triple FP isolator reached about 15 inches (when the horizontal acceleration was scaled to 0.6g and vertical acceleration scaled to 0.48g), which increased more than three times compared to far-field motions.
Also, the fragility curves show that using a three-dimensional isolation system with rocking increases the PGA_F values by more than 80% compared to the horizontal isolation only. Hence, when the transverse acceleration limit of the bushing is equal to 2g, using a three-dimensional isolation system with a more horizontal capacity of triple FP is effective in improving the seismic performance of the isolated transformer and reducing the probability of failure.

References

[1] Wilcoski J, Smith SJ. Fragility testing of a power transformer bushing –Demonstration of CERL equipment fragility and protection procedure. US Army Corps of Engineers, Construction Engineering Research Laboratories; USA-CERL Technical Report 97/57 February 1997.

[2] Gilani AS, Whittaker AS, Fenves GL, Fujisaki E. Seismic evaluation of 550 kV porcelain transformer bearings. PEER 1998/05 October. 1999, PEER, Pacific Earthquake Engineering Research Center.

[3] Gilani AS, Whittaker AS, Fenves GL, Fujisaki E. Seismic evaluation of 230 kV porcelain transformer bearings. PEER 1998/14 December. PEER, Pacific Earthquake Engineering Research Center; 1999.

[4] Filiatrault A, Matt H. Experimental seismic response of the high-voltage transformer-bushing system. Earthq Spectra 2005;21(4):1009–25.

[5] Reinhorn AM, Oikonomou K, Roh H, Schiff A, Kempner Jr L. Modeling and seismic performance evaluation of high voltage transformers and bushings [MCEER-11-0006 2011]. Buffalo, NY: Multidisciplinary Center for Earthquake Engineering Research; 2011.

[6] Shumuta Y. A study on seismic retrofit planning method of substation components on the basis of the seismic risk assessment of electric power system. CRIEPI Report U33, Japan; 1998 [in Japanese].

[7] Oikonomou K, Roh H, Reinhorn AM, Schiff A, Kempner L Jr. Seismic performance evaluation of high voltage transformer bushings. In: Proceeding of ASCE 2010 Structures Congress 2010, May 12-15; Orlando, FL.

[8] Oikonomou K, Constantinou MC, Reinhorn AM, Kempner Jr L. Seismic isolation of high voltage electrical power transformers [MCEER-16-0006 2016]. Buffalo, NY: Multidisciplinary Center for Earthquake Engineering Research; 2016.

[9] Whittaker AS, Fenves GL, Gilani ASJ. Earthquake performance of porcelain transformer bushings.Earthq Spectra 2004;20(1):205–23.

[10] Suzuki H, Sugi T, Kuwahara H, Kaizu N. Studies on aseismic isolation device for electric substation equipment. In: Cakmak AS, editor. Soil-structure interaction. Elsevier; 1987.

[11] Ersoy S, Saadeghvaziri MA, Liu GY, Mau ST. Analytical and experimental seismic studies of transformers isolated with friction pendulum systems and design aspects. Earthq Spectra 2001;17(4):569–95.

[12] Murota N, Feng MQ, Liu GY. Earthquake simulator testing of base-isolated power transformers. IEEE Trans Power Delivery 2006;21(3):1291–9.

[13] Koliou M, Filiatrault A, Reinhorn AM. Seismic response of high-voltage transformer-bushing systems incorporating flexural stiffeners I: Numerical study. Earthq Spectra 2013;29(4):1335–52.

[14] Zou D, Zhao L, He C, Xie Q . (2021). Seismic Performance of ±800 kV Ultra-High Voltage Converter Transformer-Bushing System, Conference: 2021 International Conference on Electrical Materials and Power Equipment (ICEMPE).

[15] Ma G, Xie Q, Whittaker A . (2019). Seismic Performance Assessment of an Ultra-High–Voltage Power Transformer, Earthquake Spectra 35(1):423_435.

[16] Shen L, Li H, Duan Y . (2021). Seismic Performance and Vulnerability Analysis of High Voltage Capacitor, 2021 Power System and Green Energy Conference (PSGEC).

[17] Kitayama S, Constantinou MC, Lee D. (2016). Procedures and results of the assessment of the seismic performance of seismically isolated electrical transformers with due consideration for vertical isolation and vertical ground motion effects. Report *MCEER-16-0010*. Multidisciplinary Center for Earthquake Engineering Research, Buffalo, NY.

[18] Kitayama S, Lee D, Constantinou MC and Kempner L. (2017). Probabilistic seismic assessment of seismically isolated electrical transformers considering vertical isolation and vertical ground motion. Engineering Structures, 152 (1), pp. 888-900.

[19] FEMA (2009). "Quantification of Building Seismic Performance Factors" *Report FEMA P695*, Federal Emergency Management Agency, Washington, DC.

[20] American Society of Civil Engineers (ASCE) (2017). Standard ASCE/SEI 7-16, Minimum design loads for buildings and other structures, Reston, VA.

[21] Kitayama S and Constantinou MC.(2020).Further Results on the Assessment of Performance of Seismically Isolated Electrical Transformers, Report MCEER-20-0002, Multidisciplinary Center for Earthquake Engineering Research, Buffalo, NY.

[22] Kitayama, S and Constantinou, MC. (2019a). Probabilistic seismic performance assessment of seismically isolated buildings designed by the procedures of ASCE/SEI 7 and other enhanced criteria. Engineering Structures, 179, pp. 566-582.

[23] Kitayama, S and Constantinou, MC. (2019b). Effect of displacement restraint on the collapse performance of seismically isolated buildings. Bulletin of Earthquake Engineering, https://doi.org/10.1007/s10518-019-00626-z.

[24] Vamvatsikos D, Cornell CA. Incremental dynamic analysis. Earthq Eng Struct Dynam 2002;31(3):491–514. https://doi.org/10.1002/eqe.141.

[25] Anagnos T. Development of an electrical substation equipment performance database for evaluation of equipment fragilities. Report PEER Report 2001/06, Pacific Earthquake

Engineering Research Center, University of California, Berkeley, CA.

[26] Kempner L Jr, Eidinger J, Perez J, Schiff A. Seismic risk of high voltage electric transmission network. In: 8th US National Conference on Earthquake Engineering 2006; April 18–22, San Francisco, CA.

[27] Ostrom D. SERAII. Advancing mitigation technologies and disaster response for lifeline systems 2003, ASCE, pp. 587–596, DOI: https://doi.org/10.1061/40687 (2003)60.

[28] Ostrom D. Database of seismic parameters of equipment in substations. PEER Lifelines Task 413 Final Report 2004; July, PEER Center College of Engineering, University of California, Berkeley, CA.

[29] Kumar M., Whittaker A. S., Constantinou M. C. (2014). "Characterizing Friction in Sliding Isolation Bearings." *Earthquake Engineering and Structural Dynamics*, **44** (9): 1409–1425.

[30] Haselton C. B. (2006). "Assessing Seismic Collapse Safety of Modern Reinforced Concrete Moment Frame Buildings" *Ph.D. Thesis*, Department of Civil and Environmental Engineering, Stanford University, Palo Alto, CA.

[31] Haselton C. B., Deierlein G. G. (2007). "Assessing Seismic Collapse Safety of Modern Reinforced Concrete Frame Buildings" *Blume Earthquake Engineering Research Center Technical Report No. 156*, Stanford University, Palo Alto, CA.

[32] Haselton C. B., Mitrani-Reiser J., Goulet C. A., Deierlein G. G., Beck J. L., Porter K. A., Stewart J. P., Taciroglu E. (2008). "An Assessment to Benchmark the Seismic Performance of a Code-Conforming Reinforced-Concrete Moment-Frame Building." *Report PEER Report 2007/12*, Pacific Earthquake Engineering Research Center, University of California, Berkeley, CA.

[33] Liel A. B., Haselton C. B., Deierlein G. G. (2011). "Seismic Collapse Safety of Reinforced Concrete Buildings: II. Comparative Assessment of Non-Ductile and Ductile Moment Frames." *Journal of Structural Engineering* **134** (7): 492-502.

[34] Lignos D., Krawinkler H. (2013). "Sideways Collapse of Deteriorating Structural Systems under Seismic Excitations." *Blume Earthquake Engineering Research Center Technical Report No. 177*, Stanford University, Palo Alto, CA.

[35] Medina R. A., Krawinkler H. (2004). "Seismic Demands for Nondeteriorating Structures and Their Dependence on Ground Motions." Report MEER Report 2003/15, Pacific Earthquake Engineering Research Center College of the Engineering University of California, Berkeley, CA.

[36] Institute of Electrical and Electronics Engineers (IEEE) (2005). "IEEE Recommended Practice for Seismic Design of Substations, IEEE Standard 693." IEEE Power Engineering Society, The Institute of Electrical and Electronics Engineers, Inc., New York, NY.

[37] Shinozuka M., Dong X., Chen T. C., Jin X. (2007). "Seismic Performance of Electric Transmission Network under Component Failures." *Earthquake Engineering and Structural Dynamics*; **36**: 227-244.

[38] Kitayama S and Constantinou MC. (2018a). Seismic Performance assessment of seismically isolated buildings designed by the procedures of ASCE/SEI 7. Report MCEER-18-0004, Multidisciplinary Center for Earthquake Engineering Research, Buffalo, NY.

[39] Kitayama S and Constantinou MC. (2018b). Collapse performance of seismically isolated buildings designed by the procedures of ASCE/SEI 7. Engineering Structures, 164, pp. 243-258.

[40] Kempner L. Jr., Eidinger J., Perez J., Schiff A. (2006). "Seismic Risk of High Voltage Electric Transmission Network." *8th U.S. National Conference on Earthquake Engineering*, April 18-22, San Francisco, CA.

[41] Shumuta Y. (2007). "Practical Seismic Upgrade Strategy for Substation Equipment based on Performance Indices." *Earthquake Engineering and Structural Dynamics*, **27**(2): 209-226.

[42] Kong D. (2010). "Evaluation and Protection of High Voltage Electrical Equipment against Severe Shock and Vibrations." *Ph.D. Thesis*, University at Buffalo, State University of New York, Buffalo, NY.

[43] Fahad M. (2013). "Seismic Evaluation and Qualification of Transformer Bushings." *Ph.D. Thesis*, University at Buffalo, State University of New York, Buffalo, NY.

[44] Villaverde R, Pardoen GC, Carnalla S. Ground motion amplification at flange level of bushings mounted on electric substation transformers. Earthq Eng Struct Dynam 2001;30(5):621–32.

[45] Fenz DM, Constantinou MC. Development, implementation, and verification of dynamic analysis models for multi-spherical sliding bearings. MCEER-08-0018 2008; Multidisciplinary Center for Earthquake Engineering Research, Buffalo, NY.

[46] Sarlis AA, Constantinou MC. Shake table testing of triple friction pendulum isolators under extreme conditions. MCEER-13-0011 2013; Multidisciplinary Center for Earthquake Engineering Research, Buffalo, NY.

[47] McKenna F. T. (1997). "Object-Oriented Finite Element Programming: Frameworks for Analysis, Algorithms and Parallel Computing." *Ph.D. Thesis*, Department of Civil and Environmental Engineering, University of California, Berkeley, CA.

[48] McVitty WJ, Constantinou MC. Property modification factors for seismic isolators: design guidance for buildings. MCEER-15-0005; Multidisciplinary Center for Earthquake Engineering Research, Buffalo, NY.

[49] PEER NGA WEST 2 <http://ngawest2.berkeley.edu/> [9 November 2015].

[50] Khansefid, A., 2020. Pulse-like ground motions: Statistical characteristics, and GMPE development for the Iranian Plateau. Soil Dynamics and Earthquake Engineering, 134, p.106164.

[51] Somerville, P.G., 2003. Magnitude scaling of the near fault rupture directivity pulse. Physics of the earth and planetary interiors, 137(1-4), pp.201-212.

[52] Huang, Y.N., Whittaker, A.S. and Luco, N., 2008. Maximum spectral demands in the near-fault region. Earthquake Spectra, 24(1), pp.319-341.

[53] Almufti, I., Motamed, R., Grant, D.N. and Willford, M., 2015. Incorporation of velocity pulses in design ground motions for response history analysis using a probabilistic framework. Earthquake Spectra, 31(3), pp.1647-1666.

[54] Sokolov A, Shadrikov T. (2021). Method for Calculating Increased Frequency High-Voltage Power Transformer, 2021 International Ural Conference on Electrical Power Engineering.

[55] Lee D, Constantinou MC . (2018). Combined horizontal–vertical seismic isolation system for high-voltage–power transformers: development, testing, and validation, Bulletin of Earthquake Engineering 16(2).